



## Atomic and electronic structures of nitrogen vacancies in silicon nitride: Emergence of floating gap states

Fugo Nanataki,<sup>1</sup> Kenji Shiraishi <sup>1,2,\*</sup> Jun-ichi Iwata,<sup>3,4</sup> Yu-ichiro Matsushita,<sup>3,4</sup> and Atsushi Oshiyama <sup>2,†</sup>

<sup>1</sup>Graduate School of Engineering, Nagoya University, Furo, Chikusa, Nagoya, 464-8603, Japan

<sup>2</sup>Institute of Materials and Systems for Sustainability, Nagoya University, Furo, Chikusa, Nagoya 464-8601, Japan

<sup>3</sup>Quemix Inc., Nihonbashi, Chuo, Tokyo 103-0027, Japan

<sup>4</sup>Tokyo Institute of Technology, Ohokayama, Meguro, Tokyo 152-8550, Japan



(Received 11 August 2022; revised 8 September 2022; accepted 11 October 2022; published 25 October 2022)

We report the density functional calculations with the hybrid approximation to the exchange-correlation energy that clarify the atomic and electronic structures of the N vacancy ( $V_N$ ) in  $Si_3N_4$ . We find that the gap states induced by the Si dangling bonds around  $V_N$  show interesting interplay between the spin splitting and the Jahn-Teller splitting depending on their charges. More surprisingly, we find that a peculiar electron state distributed in the internal space of the host SiN is hidden in the conduction bands and converted to a localized floating state in the fundamental energy gap due to the presence of  $V_N$ . This theoretical finding indicates  $V_N$  being multiply charged from +1 to -5: The charge states from +1 to -3 are stable at respective Fermi-level positions in the gap, whereas the states -4 and -5 are metastable for the Fermi level near the conduction band bottom. A possibility of multilevel memory function of  $V_N$  in SiN is suggested.

DOI: [10.1103/PhysRevB.106.155201](https://doi.org/10.1103/PhysRevB.106.155201)

### I. INTRODUCTION

Defects inevitably existing in materials affect the properties of the materials substantially. Point defects in semiconductors or insulators induce electron states in fundamental energy gaps (deep or shallow levels) of the host materials, and the induced states capture or emit electrons in relatively localized regions. [1–3]. Such point defects affect the transport and optical properties, thus occasionally leading to deterioration of electron devices. However, capturing and/or emitting the charge in a rather localized region exactly corresponds to storing information in the region. If one can control the capture and emission of the point defect, it is utilized as an ultimately miniaturized element in technology. Such a case is extremely rare in history but now emerging: The nonvolatile flash memory [4] which sustains our current lives is an example. Upon miniaturization of the electron devices, the memory element of such a flash previously composed of Si floating gates is now succeeded by silicon nitride (SiN) placed near the interface of metal-oxide-semiconductor structures [5,6]. The memory function of SiN is supposed to come from the nitrogen vacancy ( $V_N$ ) [7–10], although its mechanism is unknown. Hence, clarifying the atomic and electronic structures of  $V_N$  in SiN is inevitable from both science and technology viewpoints.

SiN is a useful material under harsh environments due to its high thermal stability and toughness against fracture [11] and lately has been utilized as passivation layers in Si solar cells [12]. In pioneering tight-binding calculations by Robertson and Powell [13] and Robertson [14], it was shown that the material in its stable stoichiometry  $Si_3N_4$  is a semiconductor

with the valence band top (VBT) being the N lone pairs, and several point defects are classified based on the obtained chemical knowledge. This classification is essentially correct and has been corroborated by recent calculations based on density functional theory (DFT) [15].

To advance our understanding of the memory function in SiN, however, the most important task is the determination of the thermodynamic (TD) level [16,17] induced by  $V_N$ ,  $\varepsilon(q|q')$ , i.e., the determination of the Fermi level in the gap at which differently charged  $V_N$ , i.e.,  $V_N^q$  and  $V_N^{q'}$ , have the same total energy. This TD level is responsible for the electron capture and emission, and its determination involves assessment of roles of hybridization, spin polarization and ionicity of  $V_N$  in SiN, which we clarify in this paper.

Another important factor discussed in this paper is the role of spatial sparsity of the material in its electronic properties. In carbon nanomaterials such as tubes or peapods [18–20], there are internal hollows where peculiar electron states are distributed and affect the electronic properties substantially [21,22]. Even in typical tetrahedrally coordinated semiconductors which show relatively low packing efficiency compared with metals, there are electron states which are distributed in the interstitial channels [23,24], and the quantum confinement of the electron in the interstitial channel nicely explains the bandgap variation among polymorphs of silicon carbides [25,26]. In this paper, we find this class of the peculiar electron state, which we call a *floating state*, is hidden in the host SiN as a conduction band state and emerges as a gap state due to the presence of the N vacancy. This emergence of the new TD levels renders  $V_N$  a multiply charged system, opening its possibility as a promising memory unit in information technology.

In Sec. II, the present calculation schemes are explained. The floating states in defect-free SiN which we have found

\*shiraishi@imass.nagoya-u.ac.jp

†oshiyama@imass.nagoya-u.ac.jp

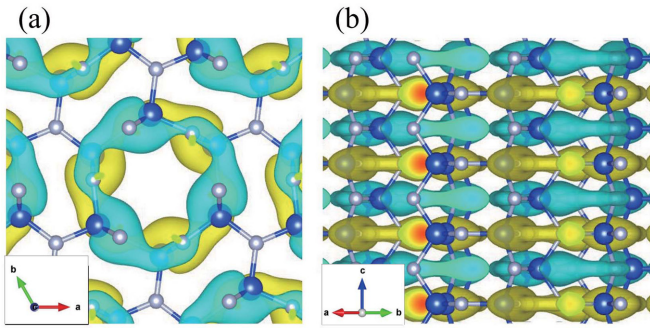


FIG. 1. Kohn-Sham (KS) orbital of the bottom of the conduction band at the  $\Gamma$  point of  $\beta$ - $\text{Si}_3\text{N}_4$  obtained by the hybrid approximation of Heyd-Scuseria-Ernzerhof (HSE), viewed (a) from the  $c$  axis and (b) from its perpendicular direction. The isovalue surface of the KS orbital is shown by the yellow (+) and blue-green (−) blobs. The absolute value of the isovalue is 30% of the maximum. The blue and gray balls depict Si and N atoms, respectively.

are presented in Sec. III A, and the emergence of various gap states induced by  $V_N$  and their characters are discussed in Sec. III B. Section IV summarizes our findings.

## II. CALCULATIONS

Calculations have been done in DFT [27,28] using either our own real-space-scheme code RSDFT [29,30] or the plane-wave-scheme code VASP [31,32]. The results obtained by the two different codes are essentially identical and thus confirm the validity. The generalized gradient approximation (GGA) of Perdew-Burke-Ernzerhof (PBE) [33] is used to determine the stable geometries, and the total energies with various charge states (i.e., the determination of the TD levels) with appropriate corrections in the charged supercell calculations [34–37] are obtained by the hybrid approximation of Heyd-Scuseria-Ernzerhof (HSE) [38,39], using the geometries obtained by GGA-PBE. As a representative of SiN, we take crystalline  $\beta$ - $\text{Si}_3\text{N}_4$ , and to simulate a single  $V_N$  in an otherwise perfect  $\beta$ - $\text{Si}_3\text{N}_4$ , the 224-site supercell (and the 756-site supercell for the examination of the validity) is used. More details are explained in Appendix A.

## III. RESULTS AND DISCUSSION

### A. Floating state in perfect SiN

In  $\beta$ - $\text{Si}_3\text{N}_4$ , Si is fourfold coordinated with N, and N is threefold coordinated with Si. We have confirmed that the VBT has a character of N lone pairs. For the conduction band state, however, we have found that it lacks such a chemical interpretation. Figure 1 is the Kohn-Sham (KS) orbital of the conduction band bottom (CBB), clearly showing that this state is distributed neither around the atoms nor along the bond network: Its amplitude is the highest in the interstitial region behind the Si-N bonds [larger electron blobs in Fig. 1(a)] and then extended along the hexagonal rings, forming a floating shape in the internal space of  $\text{Si}_3\text{N}_4$ . From the direction perpendicular to the  $c$  axis, i.e., along the hexagonal ring plane [Fig. 1(b)], nodal planes are observed. This nodal plane comes from the requirement of the orthogonalization

TABLE I. The Si-Si distances in Å,  $d_{12}$ ,  $d_{23}$ , and  $d_{31}$ , among 3 Si atoms which surround  $V_N$  for various charge states obtained by the geometry optimization using GGA-PBE. The numbering of the 3 Si atoms are shown in Fig. 9 in Appendix C. The corresponding distances in vacancy-free  $\text{Si}_3\text{N}_4$  are shown at the last column. The values for  $V_N$  at site B are also shown in parentheses.

	$V_N^+$	$V_N^0$	$V_N^-$	$V_N^{2-}$	$V_N^{3-}$	$V_N^{4-}$	$V_N^{5-}$	xtal
$d_{12}$	3.17 (3.02)	2.78 (2.73)	2.53 (2.49)	2.89 (2.50)	2.46 (2.49)	2.36 (2.39)	2.47 (2.33)	3.07 (3.02)
$d_{23}$	2.90 (3.02)	3.01 (2.72)	3.03 (2.45)	2.49 (2.47)	2.54 (2.49)	2.40 (2.39)	2.30 (2.33)	2.92 (3.02)
$d_{31}$	3.17 (3.02)	2.78 (3.12)	2.53 (3.15)	2.46 (2.84)	2.46 (2.49)	2.36 (2.39)	2.47 (2.33)	3.07 (3.02)

with the occupied  $sp$  hybridized orbitals of Si and N. The appearance of such a floating state is common to sparse materials, as stated in Sec. I: Our DFT calculations for carbon nanotubes [21], carbon peapods [22], and even for typical semiconductors [23–26] have predicted the appearance of the floating states, and the present calculation adds an interesting member of those sparse materials. The packing efficiency of  $\beta$ - $\text{Si}_3\text{N}_4$  is 0.28, which is lower than the value 0.34 of typical semiconductors.

### B. Nitrogen vacancy

In a unit cell of  $\beta$ - $\text{Si}_3\text{N}_4$ , there are 6 Si and 8 N atoms, and the 8 N sites are classified into inequivalent two groups: the majority 6 sites (site A hereafter) and the minority 2 sites (site B hereafter). The formation energies of neutral  $V_N$  at the two distinct sites have been calculated and found to be close to each other within 0.1 eV. Here, we present the results mainly for  $V_N$  at site A. The results for site B are generally same as those for the majority site but show interesting differences in some aspects (see below). Detailed results for site B are presented in Appendix B.

Three Si atoms around an N atom in  $\beta$ - $\text{Si}_3\text{N}_4$  form an equilateral (site B) or isosceles (site A) triangle. The length difference in the isosceles triangle is 2.5%. The geometry of the three Si atoms labeled Si(1), Si(2), and Si(3) are shown in Fig. 9 in Appendix C. The distance  $d_{ij}$  between Si( $i$ ) and Si( $j$ ) is calculated and shown in the last column of Table I. Removing the N atom induces dangling bonds of those 3 Si atoms, inducing localized electron states near the gap. In the unrelaxed geometry, the point-group symmetry of  $V_N$  is almost  $C_{3v}$ . Then the three dangling-bond states are transformed to be a single totally symmetric state (commonly called  $a_1$  state) and two almost degenerate states ( $e_1$  with its nodal plane between the base 2 Si and the top Si and  $e_2$  with the nodal plane crossing the top Si). We have found that  $a_1$  is resonant in the valence bands being located at 1.2 eV below the VBT, and  $e_1$  and  $e_2$  are located in the gap, as shown in the KS levels of  $V_N^{+1}$  in Figs. 2 and 7 in Appendix B. (The KS levels qualitatively correspond to the TD levels in usual cases.) The KS orbitals for these  $e_1$  and  $e_2$  states are shown in Fig. 3. They are empty for  $V_N^+$  and, upon electron capture, exhibit interesting competition between the Jahn-Teller (JT) and the exchange splitting. For  $V_N^0$ , an electron is accommodated in the  $e_1$  state

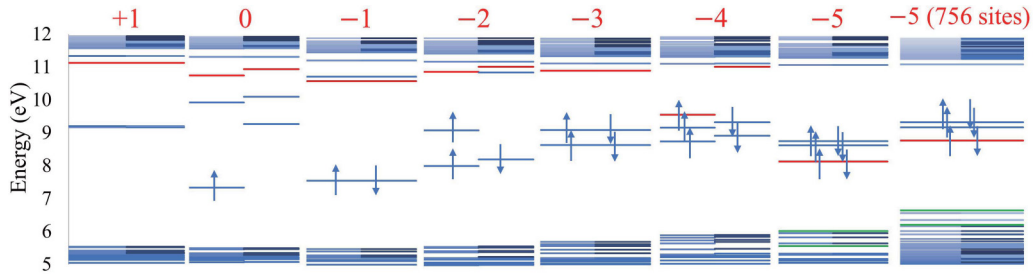


FIG. 2. Kohn-Sham levels induced by the N vacancy at site A with charge  $q$  (shown by red letters above), obtained by the hybrid approximation of Heyd-Scuseria-Ernzerhof (HSE). The blue bars  $<6$  eV and  $>11$  eV correspond to the valence and conduction bands, respectively. The lowest state of the conduction bands has the floating character as shown in Fig. 1. Other blue bars are gap states with the Si dangling-bond characters. The red bars are newly found localized floating states (see text). The green bars for the  $-5$  charge state are originated from the undercoordinated N atom (see text). The results using the 756-site supercell for  $V_N^{-5}$  are also shown.

since the neighboring 3 Si atoms form a slightly (4%) flattened isosceles triangle. This electron capture induces the exchange splitting of 1.92 eV (Fig. 2) which is substantially larger than the typical spin splitting in covalent systems such as the Si dangling bond in crystalline Si (a few tenths of electronvolts) or on the Si surface (0.79 eV [40]). This is the manifestation of the localization of the Si orbitals in  $\text{Si}_3\text{N}_4$ , reflecting an ionic character of silicon nitride. With respect to the center of mass position of  $e_1$  with up and down spins, the separation between  $e_1$  and  $e_2$  is 1.71 eV (Fig. 2) which is the JT splitting in this system. For  $V_N^{-1}$ , two electrons are accommodated in the  $e_1$  state; thus, the JT splitting becomes double of the neutral case, 3.03 eV (Fig. 2).

An additional electron is accommodated in the  $e_2$  state in  $V_N^{-2}$ . The splitting between  $e_1$  and  $e_2$  for the up spin in Fig. 2 is the crystal-field (isosceles triangle field) splitting. The exchange splitting is again prominent, and its value is 1.76 eV (Fig. 2). This value is smaller than the value for  $e_1$ , showing less localization of the  $e_2$  state. Further accommodation of an electron makes  $V_N$  triply negative, where the  $e_1$  and  $e_2$  states are fully occupied. Here, we have found that the covalency (the JT splitting) and the ionicity (the exchange splitting) become prominent alternately, depending on the number of electrons trapped in  $V_N$ . The total energies for the spin-

polarized states are lower in energy than the spin-unpolarized states by 0.43 and 0.36 eV for  $V_N^0$  and  $V_N^{2-}$ , respectively.

The floating state originating from the sparsity of  $\text{Si}_3\text{N}_4$  creates another gap state in  $V_N$ . This gap state accommodates further two electrons and renders  $V_N$  as  $-4$  and  $-5$  charge states. The energy-level position of this state is shown by the red bars in Fig. 2 for various charge states. The corresponding KS orbital is shown in Fig. 4 for the neutral and  $-5$  charge state. It does not have any particular atomic-orbital character but has the floating-state character. The floating state hidden in the conduction bands (Fig. 1) is subject to the multiple scattering by  $V_N$  and localized in the N-deficit region associated with the downward shift of its energy level: the localized floating state. The downward shift is due to the fact that the N-deficit region in ionic  $\text{Si}_3\text{N}_4$  is intrinsically positive: Our Bader charge analyses [41,42] have indeed shown its ionicity as  $\text{Si}_3^{+3.00}\text{N}_4^{-2.25}$ . Figure 4 clearly shows that this state is distributed above and below the nodal plane on the triangle of the three neighboring Si atoms (right panels of Fig. 4), like a  $\pi$  state. However, this localized floating state is not a conventional  $\pi$  state since the surrounding Si atoms are already fourfold coordinated and no atomic orbitals are available to form this state. The floating states hidden in the conduction bands have become this state due to the N vacancy. The emergence of this localized floating state is reflected on the reduction of the Si triangle in the  $-4$  and  $-5$  charge states (Table I): The Si-Si distances are comparable or even smaller than the bond length of crystalline Si (2.35 Å). It is of note that this localized floating state in  $V_N^{-4}$  shows the spin splitting of 1.46 eV, sizably smaller than that for the dangling-bond states in  $V_N^0$  and  $V_N^{-2}$ .

We have repeated the calculations using the 756-site supercell. The obtained KS levels for  $V_N^{-5}$  are shown in the last panel of Fig. 2. The results from the 756-site cell are essentially the same as those from the 224-site cell. The emergence of the floating-character gap states is common to the two distinct supercell sizes, although small KS-level shifts presumably due to the electrostatic potential shift are observed. The corresponding localized floating-state orbital from the 756-site supercell is shown in Fig. 4(c). Again the results from the two distinct supercells are essentially identical. Hence, we conclude that the emergence of the localized floating state in the gap with electrons accommodated is the real phenomenon in SiN.

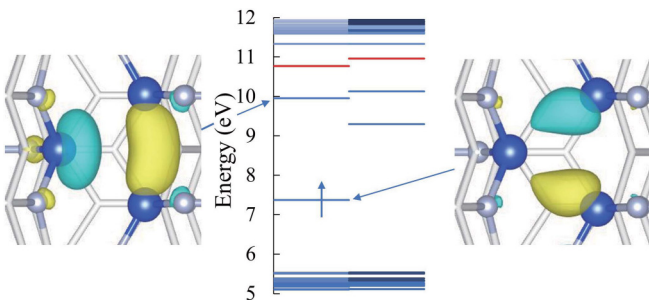


FIG. 3. Kohn-Sham (KS) orbitals of the gap states  $e_1$  (left) and  $e_2$  (right) induced by neutral N vacancy in  $\beta\text{-Si}_3\text{N}_4$ , obtained by the hybrid approximation of Heyd-Scuseria-Ernzerhof (HSE). The isovalue surfaces with the absolute value being 50% of its maximum are shown by blobs. The blue-green and the yellow blobs represent the sign of the isovalue. The blue and gray balls depict Si and N atoms, respectively.



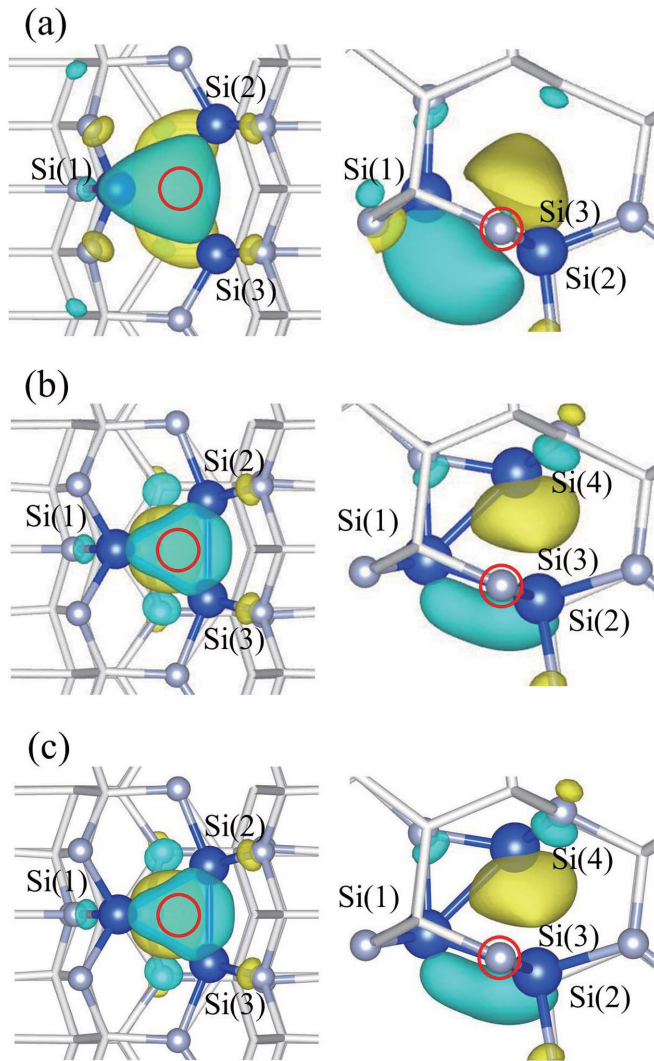


FIG. 4. Kohn-Sham orbitals obtained by the hybrid approximation of Heyd-Scuseria-Ernzerhof (HSE) of the localized floating states in the gap denoted by red bars in Fig. 2 for (a) neutral  $V_N$  and (b)  $V_N^{-5}$ , viewed from two distinct directions. The obtained localized floating-state orbital for  $V_N^{-5}$  using the 756-site supercell is also shown in (c). The isovalue surfaces of the KS orbitals are shown by yellow (+) and blue-green (−) blobs. The absolute value of the isovalue is  $\sim 50\%$  of the maximum. The blue and the gray balls depict Si and N atoms, respectively. The red circles depict the position of  $V_N$ .

In the quintuply charged vacancy  $V_N^{-5}$ , the localized floating state shifts downward substantially, becoming the lowest gap state. This is associated with spontaneous structural transformation shown in Fig. 5: One of the Si atoms second nearest to the  $V_N$  site [labeled Si(4) in Figs. 5 and 9 in Appendix C] is dislodged from its original site by cutting one of the original 4 Si-N bonds and approaches one of the nearest neighbor Si [Si(1)] of  $V_N$ , keeping its threefold coordinated geometry. The resulting Si dangling bond directed to the  $V_N$  site hybridizes with the localized floating state being already there and causes the downward shift of the hybridized state. This structural transformation is essentially the Si movement along the direction reverse to one of the 4  $sp^3$  directions, leaving

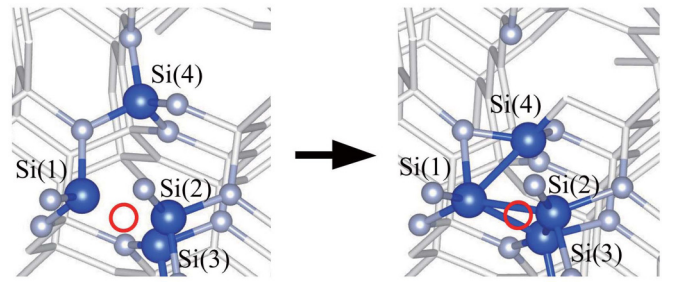


FIG. 5. Structural transformation around  $V_N^{-5}$ . An original geometry of  $V_N$  (left panel) is transformed to a puckered geometry (right panel) upon electron injection. The four Si atoms involved in this transformation are labeled. The blue and gray balls depict Si and N atoms.

the ex-partner N twofold coordinated (Fig. 5). [The twofold coordinated N induces the states in the VBT (Fig. 2).] The resulting structure is like the carrier-injected oxygen vacancy in  $\text{SiO}_2$  which is commonly called a *puckered geometry* [43–47] and has been discussed as an origin of the leakage current in the  $\text{SiO}_2$  gate insulator [47,48]. The spontaneous structural transformation found in the present calculations for  $V_N^{-5}$  elucidates the common feature between Si nitrides and oxides.

To determine which charge state of the N vacancy is favorable quantitatively, we need to calculate the formation energy of  $V_N^q$  as a function of the Fermi level ( $E_F$ ) position in the energy gap. Figure 6 is the result from the present HSE calculations. We have found a variety of charge states from +1 to  $-5$ :  $V_N^{-1}$ ,  $V_N^0$ ,  $V_N^{-1}$ ,  $V_N^{-2}$ , and  $V_N^{-3}$  appear as the ground states at the respective range of the  $E_F$  position. Here,  $V_N^{-4}$  and  $V_N^{-5}$  appear as the metastable states with their energies of a few tenths of electronvolts being higher than that of  $V_N^{-3}$  for the  $E_F$  position close to the CBB. This relatively small energy increase indicates that, if the  $E_F$  position is controlled to be near the CBB,  $V_N^{-4}$  and  $V_N^{-5}$  exist thermally with a certain portion and are accessible by the electron injection or the

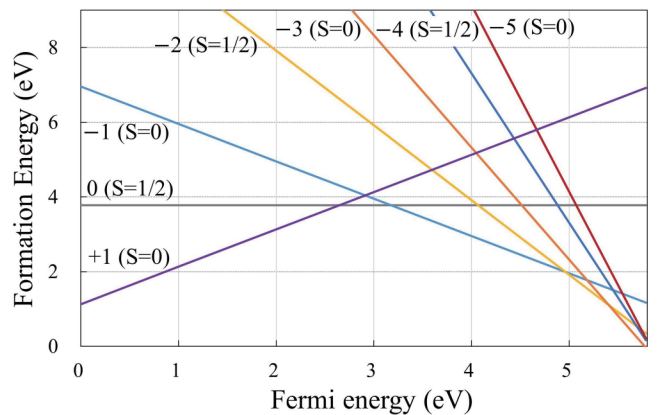


FIG. 6. Formation energy of the N vacancy with various charge states from +1 to  $-5$  as a function of the Fermi-level position in the gap of  $\beta\text{-Si}_3\text{N}_4$  obtained by the present Heyd-Scuseria-Ernzerhof (HSE) calculations. The left and right ends correspond to valence band top (VBT) and conduction band bottom (CBB), respectively. The charge and the spin  $S$  are shown near the lines.

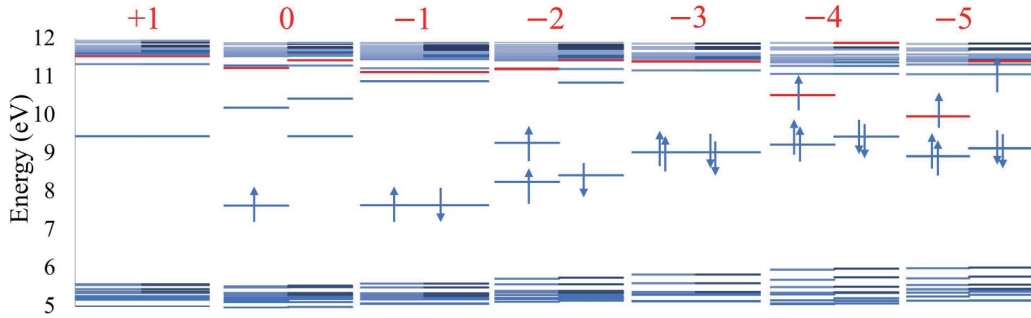


FIG. 7. Kohn-Sham levels induced by the N vacancy at site B with charge  $q$  which is shown by the number above each panel, obtained by the present Heyd-Scuseria-Ernzerhof (HSE) calculations. The blue bars  $<6$  eV and  $>11$  eV correspond to the valence and conduction bands, respectively. The lowest state of the conduction bands has the floating character as shown in Fig. 1. Other blue bars are gap states with the Si dangling-bond characters. The red bars are newly found localized floating states (see text).

infrared excitation. The obtained TD levels are  $\varepsilon (+1/0) = 2.65$  eV,  $\varepsilon (0/-1) = 3.18$  eV,  $\varepsilon (-1/-2) = 4.97$  eV, and  $\varepsilon (-2/-3) = 5.41$  eV. Figures 2 and 6 show that the N vacancy behaves as a paramagnetic center with  $S = \frac{1}{2}$  when the Fermi level is at the midgap ( $V_N^0$ ) or near the CBB ( $V_N^{-2}$  and  $V_N^{-4}$  as a metastable center).

The N vacancy  $V_N$  at the minority site B shows essentially identical behavior to that of  $V_N$  at site A (see Appendix B for details): The charge states from +1 to  $-5$  are possible due to the electron occupation of the Si dangling-bond states and also of the localized floating state. The only difference is the absence of the spontaneous structural transformation for  $V_N^{-5}$ . The reason is the geometric hindrance to the puckered configuration near  $V_N$  at site B (Figs. 7 and 9 in Appendices).

In SiN used in the flash memory, the concentration of the N vacancy is speculated to reach  $10^{19}$   $\text{cm}^{-3}$  [5,6]. The present calculations show that those vacancies are expected to be negatively charged. This leads to a possible realization of the subnanometer-scale zero-dimensional array of negatively charged quantum dots. The negative charge accommodated in the gap states is utilized to store the information. At the same

time, the negatively charged array of the dots cause the bending of the conduction and valence bands locally. This is the zero-dimensional version of the type-II superlattice. The KS levels shown in Figs. 2 and 7 for the  $-4$  and  $-5$  charge states already support this possibility: The levels corresponding to the valence bands shift upward due to the accumulation of additional electrons around the N vacancy.

#### IV. CONCLUSIONS

In summary, we have performed density functional calculations with the hybrid approximation to the exchange-correlation energy functional that clarify the atomic and electronic structures of the N vacancy ( $V_N$ ) in  $\text{Si}_3\text{N}_4$ , which is a key material in flash-memory technology. We have found

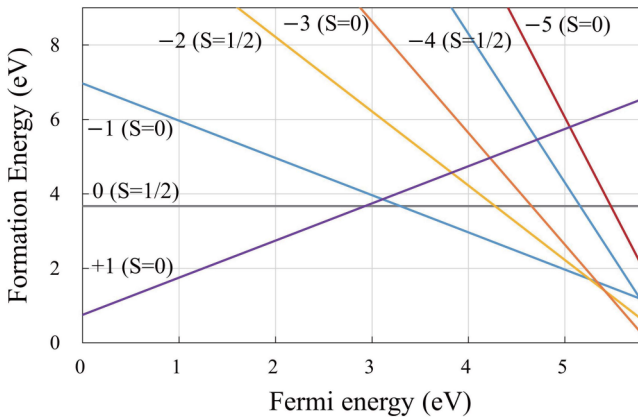


FIG. 8. Formation energy of the N vacancy at the site B with various charge states from +1 to  $-5$  as a function of the Fermi-level position in the gap of  $\beta$ - $\text{Si}_3\text{N}_4$  obtained by the present Heyd-Scuseria-Ernzerhof (HSE) calculations. The left and right ends correspond to valence band top (VBT) and conduction band bottom (CBB), respectively. The charge and the spin  $S$  are shown near the lines.

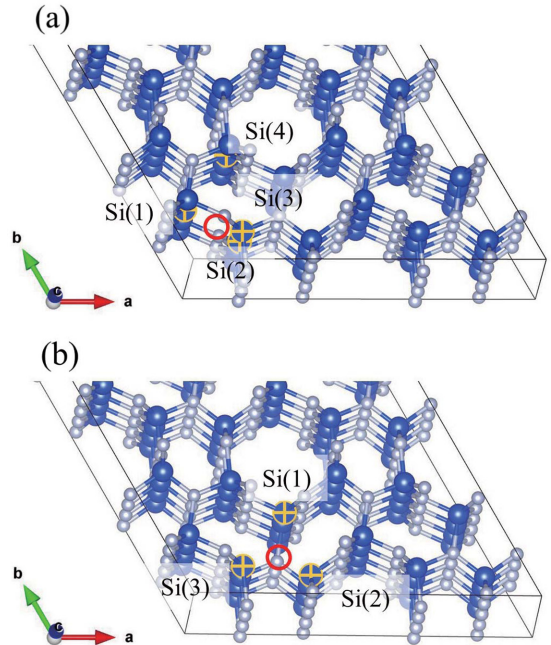


FIG. 9. Atomic structures around the N vacancy at (a) site A and (b) site B. The blue and gray balls depict Si and N atoms, respectively. The three nearest neighbor Si atoms to the N-vacancy site shown by the red circle, Si(1), Si(2), and Si(3), and the second neighbor Si [Si(4)] to the N vacancy are labeled.

that the floating state which is distributed in the internal space in the host sparse material is hidden in the conduction bands and creates a new localized floating state due to the presence of  $V_N$ . This state is unprecedented in the sense that it is distributed not around atomic sites but in the internal space of the material. This finding in addition to the quantitative clarification performed here of the dangling-bond characters has unveiled essential features of the electronic structure of the N vacancy in SiN. The calculated results indicate that  $V_N$  in SiN exhibits multiple charge states from +1 to -5: The charge states from +1 to -3 are thermodynamically stable at respective Fermi-level positions in the gap, whereas the states -4 and -5 are metastable for the Fermi level near to CBB. This multiplicity may be utilized as a multilevel memory cell in information technology.

### ACKNOWLEDGMENTS

This paper was supported by the projects conducted under MEXT Japan named “Program for Promoting Research on the Supercomputer Fugaku: Multiscale simulations based on quantum theory toward the developments of energy-saving next-generation semiconductor devices” (Project ID No. JPMXP1020200205), and “Program for research and development of next-generation semiconductor to realize energy-saving society” (Project ID No. JPI005357). This paper was also supported by the grants-in-aid from MEXT under Contract No. 18H03873. Computations were performed at the Supercomputer Center, ISSP, The University of Tokyo, and the Research Center for Computational Science, the National Institute of Natural Sciences, and also with resources of “Fugaku” provided through HPCI System Research project (Project IDs No. hp200122, No. hp210170, and No. hp220168).

### APPENDIX A: DENSITY FUNCTIONAL CALCULATIONS

In this section of the Appendix, we explain details of our calculations based on DFT for  $\beta$ -Si<sub>3</sub>N<sub>4</sub> and its N vacancy. Computations have been performed either by the plane-wave-scheme code VASP [31,32] or our own real-space-scheme code RSDFT [29,30]. Geometry optimization has been performed using GGA-PBE [33] to the exchange-correlation functional. For the obtained (meta)stable geometries, we have performed self-consistent-field calculations using HSE [38], obtained the total energies for variously charged N vacancies as a function of the Fermi-level position, and then determined the TD levels in the gap. The Fock exchange operations in HSE have been carried out by a recently proposed adaptively compressed scheme [39]. In the HSE calculations, we use the parameter which separates the short- and long-range parts as  $\omega = 0.2 \text{ \AA}^{-1}$  and the mixing ratio of the exact exchange to GGA-PBE as  $\alpha = 0.25$ . These parameters for the HSE approximation along with other computation parameters given below produce the energy gap of  $\beta$ -Si<sub>3</sub>N<sub>4</sub> being 5.8 eV, which is close to the previous value of 5.98 eV by the GW approximation [49] and in the range of the experimental values (5.3 eV in Ref. [50] although not being settled among the experiments). In the VASP computations, nuclei and core electrons are simulated by the projector-augmented potentials [51], and the cutoff

energy of the plane-wave basis set is taken to be 500 eV. In the RSDFT computations, norm-conserving pseudopotentials [52] are used to simulate nuclei and cores, and the real-space mesh spacing is taken to be 0.13 Å, corresponding to the cutoff energy of 2200 eV in the plane-wave basis set (we used the fine mesh spacing to prepare converged results). One of the reasons to perform the same computations with different codes in this paper is to confirm that the two independent computations produce identical results, and we have indeed confirmed it. As a primitive example, the obtained lattice constants of  $\beta$ -Si<sub>3</sub>N<sub>4</sub> are  $a = 7.66 \text{ \AA}$  and  $c = 2.92 \text{ \AA}$ , which agree with the experimental values with the errors of +0.66% and +0.34%, respectively.

To simulate a single N vacancy  $V_N$  in an otherwise perfect  $\beta$ -Si<sub>3</sub>N<sub>4</sub>, we use a supercell consisting of 224 atomic sites. To examine the validity of the supercell size, the 756-site supercell is also used. The 756-site supercell nominally corresponds to the  $V_N$  concentration of  $1.25 \times 10^{20} \text{ cm}^{-3}$ .

The TD levels are determined by the formation energy  $E_{\text{form}}^q$  of the N vacancy with the charge  $q$ , which is given as

$$E_{\text{form}}^q = E_{\text{tot}}^{V_N^q} - E_{\text{tot}}^{\text{xtal}} + \mu_N + q(\varepsilon_{\text{VBM}}^{\text{xtal}} + \varepsilon_F) + E_{\text{cor}}.$$

Here,  $E_{\text{tot}}^{V_N^q}$  and  $E_{\text{tot}}^{\text{xtal}}$  are the total energies of the supercell with and without  $V_N^q$ , respectively,  $\mu_N$  the chemical potential of an N atom,  $\varepsilon_{\text{VBM}}^{\text{xtal}}$  the VBT of the crystal, and  $\varepsilon_F$  the Fermi energy. Also,  $E_{\text{cor}}$  is the correction for the charged supercell calculations. The correction includes electrostatic energy of the charged periodic systems and the potential shift caused by the finite-sized supercell [34–37]. The TD level  $\varepsilon(q|q')$  is obtained by the cross point of  $E_{\text{form}}^q$  and  $E_{\text{form}}^{q'}$  as a function of the Fermi level.

### APPENDIX B: NITROGEN VACANCY AT THE MINORITY SITE B

In this section, we present the results for the N vacancy at the minority site B in  $\beta$ -Si<sub>3</sub>N<sub>4</sub>. The atomic structure of  $V_N$  at site B is essentially identical to the structure at site A, as shown in Table I in the main text. The obtained KS levels induced by  $V_N$  at site B are shown in Fig. 7. The TD levels, i.e., the formation energy as a function of the Fermi-level position for various charge states, are shown in Fig. 8.

The appearance of various charge states from +1 to -5 has also been found for  $V_N$  at site B. From +1 to -3 charge states, electrons are accommodated in the states essentially consisting of the dangling bonds of nearest neighbor Si atoms. Interesting competition between the symmetry-lowering relaxation (JT effect) and the spin polarization (exchange interaction) has been found, as in  $V_N$  at site A. Electrons are accommodated in the dangling-bond-character states one by one up to the -3 charge state. As in  $V_N$  at site A, the floating state hidden in the conduction band of Si nitride induces the localized floating state in the gap with the N removal (Fig. 7).

The difference from  $V_N$  at site A has been found for the quintuply charged vacancy  $V_N^{5-}$ . No spontaneous structural transformation has been observed for  $V_N$  at site B. The reason is the geometric circumstances around the N vacancy in  $\beta$ -Si<sub>3</sub>N<sub>4</sub>. Around site B, the dislodged Si [Si(4)] is unable to find its partner Si near  $V_N$ .



We have found that, for the N vacancy at site B,  $V_N^{+1}$ ,  $V_N^0$ ,  $V_N^{-1}$ ,  $V_N^{-2}$ , and  $V_N^{-3}$  appear as the ground states in the respective range of the Fermi-level position. Here,  $V_N^{-4}$  and  $V_N^{-5}$  appear as the metastable states with their energies being 0.88 and 1.84 eV, respectively, higher than that of  $V_N^{-3}$  for the Fermi-level position close to the CBB. The obtained TD levels are  $\varepsilon (+1/0) = 2.92$  eV,  $\varepsilon (0/-1) = 3.30$  eV,  $\varepsilon (-1/-2) = 5.25$  eV, and  $\varepsilon (-2/-3) = 5.42$  eV.

### APPENDIX C: NEAREST NEIGHBOR SI ATOMS AROUND THE NITROGEN VACANCY

There are three Si atoms nearest to the N vacancy which are labeled Si(1), Si(2), and Si(3). They are shown in Fig. 9 for  $V_N$  at sites A and B. The distance  $d_{ij}$  in Table I depicts the distance between Si( $i$ ) and Si( $j$ ). The fourth Si labeled Si(4), which plays an important role in the spontaneous structural transformation in  $V_N^{-5}$  at site A, is also shown in Fig. 9(a).

- [1] *Theory of Defects in Semiconductors (Topic in Applied Physics 104)*, edited by D. A. Drabold and S. Estreicher (Springer, Berlin, Heidelberg, 2007).
- [2] *Characterization of Defects and Deep Levels for GaN Power Devices*, edited by T. Narita and T. Kachi (AIP Publishing, New York, 2020).
- [3] For recent works, *Proceedings of 31th International Conference on Defects in Semiconductors, J. Appl. Phys. Special Topics* (2022).
- [4] H. Takato, K. Sunouchi, N. Okabe, A. Nitayama, K. Hieda, F. Horiguchi, and F. Masuoka, *IEDM Tech. Dig.* 222 (1988).
- [5] T. Yaegashi, T. Okamura, W. Sakamoto, Y. Matsunaga, T. Toba, K. Sakuma, K. Gomikawa, K. Komiyama, H. Nagashima, H. Akahori *et al.*, in *2009 Symposium on VLSI Technology* (IEEE, Kyoto, 2009), pp. 190–191.
- [6] S. Tsuda, Y. Kawashima, K. Sonoda, A. Yoshitomi, T. Mihara, S. Narumi, M. Inoue, S. Muranaka, T. Maruyama, T. Yamashita *et al.*, in *2016 IEEE Electron Devices Meeting (IEDM)* (IEEE, San Francisco, 2016), pp. 11.1.1–11.1.4.
- [7] E. Vianello, L. Perniola, P. Blaise, G. Molas, J. P. Colonna, F. Driussi, P. Plestari, D. Esseni, L. Selmi, N. Rochat, *et al.*, in *2009 IEEE International Electron Devices Meeting (IEDM)* (IEEE, Baltimore, 2009), pp. 1–4.
- [8] K. Yamaguchi, A. Otake, K. Kobayashi, and K. Shiraishi, in *2009 IEEE International Electron Devices Meeting (IEDM)* (IEEE, Baltimore, 2009), pp. 1–4.
- [9] K. Yamaguchi, A. Otake, K. Kamiya, Y. Shigeta, and K. Shiraishi, in *2010 International Electron Devices Meeting* (IEEE, San Francisco, 2010), pp. 5.7.1–5.7.4.
- [10] K. Yamaguchi, A. Otake, K. Kamiya, Y. Shigeta, and K. Shiraishi, *Jpn. J. Appl. Phys.* **50**, 04DD05 (2011).
- [11] F. L. Riley, *J. Am. Ceram. Soc.* **83**, 245 (2000).
- [12] A. G. Aberle, *Sol. Energy Mater. Sol. Cells* **65**, 239 (2001).
- [13] J. Robertson and M. J. Powell, *Appl. Phys. Lett.* **44**, 415 (1984).
- [14] J. Robertson, *Phil. Mag. B* **69**, 307 (1994).
- [15] L. E. Hintzschke, C. M. Fang, M. Marsman, G. Jordan, M. W. P. E. Lamers, A. W. Weeber, and G. Kresse, *Phys. Rev. B* **88**, 155204 (2013).
- [16] G. A. Baraff, E. O. Kane, and M. Schlüter, *Phys. Rev. B* **21**, 5662 (1980).
- [17] R. Car, P. J. Kelly, A. Oshiyama, and S. T. Pantelides, *Phys. Rev. Lett.* **52**, 1814 (1984).
- [18] S. Iijima, *Nature (London)* **354**, 56 (1991).
- [19] N. Hamada, S. I. Sawada, and A. Oshiyama, *Phys. Rev. Lett.* **68**, 1579 (1992).
- [20] T. Pichler, H. Kuzmany, H. Kataura, and Y. Achiba, *Phys. Rev. Lett.* **87**, 267401 (2001).
- [21] S. Okada, A. Oshiyama, and S. Saito, *Phys. Rev. B* **62**, 7634 (2000).
- [22] S. Okada, M. Otani, and A. Oshiyama, *Phys. Rev. B* **67**, 205411 (2003).
- [23] Y. I. Matsushita, S. Furuya, and A. Oshiyama, *Phys. Rev. Lett.* **108**, 246404 (2012).
- [24] Y. I. Matsushita and A. Oshiyama, *J. Phys. Soc. Jpn.* **86**, 054702 (2017).
- [25] Y. I. Matsushita and A. Oshiyama, *Phys. Rev. Lett.* **112**, 136403 (2014).
- [26] Y. Matsushita and A. Oshiyama, *Nano Lett.* **17**, 6458 (2017).
- [27] P. Hohenberg and W. Kohn, *Phys. Rev.* **136**, B864 (1964).
- [28] W. Kohn and L. J. Sham, *Phys. Rev.* **140**, A1133 (1965).
- [29] J.-I. Iwata, D. Takahashi, A. Oshiyama, B. Boku, K. Shiraishi, S. Okada, and K. Yabana, *J. Comput. Phys.* **229**, 2339 (2010).
- [30] Y. Hasegawa, J.-I. Iwata, M. Tsuji, D. Takahashi, A. Oshiyama, K. Minami, T. Boku, H. Inoue, Y. Kitazawa, I. Miyoshi *et al.*, *Int. J. High Perform. Comput. Appl.* **28**, 335 (2014).
- [31] G. Kresse and J. Furthmüller, *Phys. Rev. B* **54**, 11169 (1996).
- [32] G. Kresse and D. Joubert, *Phys. Rev. B* **59**, 1758 (1999).
- [33] J. P. Perdew, K. Burke, and M. Ernzerhof, *Phys. Rev. Lett.* **77**, 3865 (1996).
- [34] C. Freysoldt, J. Neugebauer, and C. G. Van de Walle, *Phys. Rev. Lett.* **102**, 016402 (2009).
- [35] C. Freysoldt, J. Neugebauer, and C. G. Van de Walle, *Phys. Status Solidi B* **248**, 1067 (2011).
- [36] H.-P. Komsa, T. T. Rantala, and A. Pasquarello, *Phys. Rev. B* **86**, 045112 (2012).
- [37] Y. Kumagai and F. Oba, *Phys. Rev. B* **89**, 195205 (2014).
- [38] J. Heyd, G. E. Scuseria, and M. Ernzerhof, *J. Chem. Phys.* **118**, 8207 (2003).
- [39] L. Lin, *J. Chem. Theory Comput.* **12**, 2242 (2016).
- [40] S. Okada, K. Shiraishi, and A. Oshiyama, *Phys. Rev. Lett.* **90**, 026803 (2003).
- [41] R. F. Bader, *Atoms in Molecules: A Quantum Theory* (Oxford University Press, Oxford, 1994).
- [42] G. Henkelman, A. Arnaldsson, and H. Jónsson, *Comput. Mater. Sci.* **36**, 354 (2006).
- [43] J. K. Rudra and W. B. Fowler, *Phys. Rev. B* **35**, 8223 (1987).
- [44] K. C. Snyder and W. B. Fowler, *Phys. Rev. B* **48**, 13238 (1993).
- [45] D. C. Allan and M. P. Tetter, *J. Am. Ceram. Soc.* **73**, 3247 (1990).
- [46] M. Boero, A. Pasquarello, J. Sarnthein, and R. Car, *Phys. Rev. Lett.* **78**, 887 (1997).
- [47] A. Oshiyama, *Jpn. J. Appl. Phys.* **37**, L232 (1998).

- [48] A. Yokozawa, A. Oshiyama, Y. Miyamoto, and S. Kumashiro, in *International Electron Devices Meeting. IDEM Technical Digest* (IEEE, Washington, DC, 1997), pp. 703–706.
- [49] G. Kresse, M. Marsman, L. E. Hintzsche, and E. Flage-Larsen, *Phys. Rev. B* **85**, 045205 (2012).
- [50] F. Munakata, K. Matsuo, K. Furuya, and Y. Akimune, *Appl. Phys. Lett.* **74**, 3498 (1999).
- [51] P. E. Blöchl, *Phys. Rev. B* **50**, 17953 (1994).
- [52] N. Troullier and J. L. Martins, *Phys. Rev. B* **43**, 1993 (1991).